CFD study of hydrodynamics behavior of a vibrating fluidized bed using kinetic-frictional stress model of granular flow

Mahmood Reza Rahimi*, Nader Azizi**, Seyyed Hossein Hosseini***,†, and Goodarz Ahmadi****

*Process Intensification Lab., Department of Chemical Engineering, School of Engineering,
Yasouj University, Yasouj 75918-74831, Iran
**Department of Physics, Khoy Branch, Islamic Azad University, Khoy, Iran
***Department of Chemical Engineering, Faculty of Engineering, University of Ilam, Ilam 69315-516, Iran
****Department of Mechanical and Aeronautical Engineering, Clarkson University, Potsdam, NY 13699-5725, U.S.A.

Abstract−The hydrodynamics of a vertically vibrating fluidized bed was studied using an Eulerian-Eulerian two-fluid model (TFM) incorporating the kinetic theory of granular flow and including the frictional stress effects. Influences of frictional stresses, vibration amplitudes and frequency on behavior of the particles were studied. In the case with vertical vibration, the numerical results showed three regions of solid concentration along the bed height: a low particle concentration region near the bottom of the bed, a high concentration region in the middle of the bed, and a transition region at top of the bed. The accuracy of results was found to be closely related to the inclusion of the frictional stresses. Ability of the two-fluid model for predicting the hydrodynamics of vibrating fluidized beds was discussed and confirmed.

Key words: Vibrating Fluidized Beds, Hydrodynamic, Two-fluid Model, Kinetic Theory, Frictional Stresses, CFD

INTRODUCTION

Fluidized beds are widely used in chemical, petrochemical, and biochemical processes such as drying, mixing, chemical reactions, polymerization, combustion, and gasification. This is due to high efficiency of gas-solid contact in fluidized beds. Agglomerating (wet particles) and cohesive (Geldart C) particles cannot be fluidized due to the increased tendency of occurrence of channeling defects. Formation of stagnant regions and gas flow channeling in the bed leads to decreasing efficiency of gas-solid contacts. Some previous researchers presented application of vibrating fluidized beds (VFBs) for the fluidization of cohesive particles [1-3]. Adding vibration in the fluidized beds breaks stable gas flows within the channels that are created in the granular bed, likewise helps the granular bed to fluidize homogeneously [2,3]. VFBs have been studied in a number of earlier works [4-11]. Mantle et al. [12] used magnetic resonance imaging (MRI) to provide spatial and temporal information on the three dimensions features of VFBs. However, there has been little quantitative experimental data reported in the literature for validating the numerical models.

Numerical simulations have become quite popular for understanding the complex gas-solid flow behaviors, since they can provide information on the details of gas-solid hydrodynamics. Two different approaches are used for describing the complex gas-solid flow behaviors in fluidized beds, namely, Eulerian-Lagrangian and Eulerian-Eulerian approaches. In the Eulerian-Lagrangian or discrete element method (DEM), the continuous phase flow conditions are evaluated by using an Eulerian approach, while the individual particles trajectories are evaluated. While this approach requires less model-

ing assumption for the particulate phase, it becomes more and more computational expensive (CPU time and memory resource requirements) as the number of particles increases. Thus, this approach has limited application for analysis of dense gas-solid fluidized beds. For VFBs, several numerical studies based on Eulerian-Lagrangian approach have been reported in the literature [9-11,13]. Recently, comprehensive numerical study (DEM) was reported by Xiang et al. [14] for simulation of a VFB. Several successful DEM-based simulations for studying hydrodynamics of the gas-solid flow in different fluidization systems such as dense and dilute beds have been reported by the researchers [15-18]. Deen et al. [19] reviewed the use of discrete particle models (DPMs) for the study of the flow phenomena prevailing in fluidized beds.

Eulerian-Eulerian approach is the other method for describing the gas-solid flows. The popularity of this approach stems from the smaller CPU and memory resource requirements. In the Eulerian-Eulerian two-fluid model (TFM), the two phases are treated as interpenetrating continua. This approach has been successfully utilized for predicting and validating hydrodynamics of the gas-solid systems, e.g., Passalacqua and Marmo [20] used the TFM incorporating KTGF-frictional stresses to predict bubble diameter in a bubbling fluidized bed with a central jet and the bubble diameter distribution in a uniformly fed bubbling fluidized bed. Zhong et al. [21], Wang et al. [22], Wang et al. [23] and Pei et al. [24] applied TFM to study hydrodynamics of spout-fluid bed, fluidized bed coal gasification, circulating fluidized beds and jet fluidized beds, respectively. The success of a TFM depends on the proper description of the interfacial forces and the constitutive models for solid and fluid stresses. The interfacial forces are used to describe the momentum transfer between the phases, which significantly affects the hydrodynamic behavior of the two-phase flows.

The frictional stresses play an important role in the modeling of

---

the dense fluidization systems. Several successful simulation results for the dense gas-solid fluidization systems such as the bubbling fluidized beds, jet fluidized beds and cylindrical spouted beds using combinations of frictional and kinetic stresses have been reported in the literature [20,25-27]. Patil et al. [28,29], Passalacqua and Marmo [20] and Vun et al. [25] showed that the frictional stress influences the shape of the bubble in the bubbling fluidized beds. Hosseini et al. [30] showed that the frictional stress model significantly affected the accuracy of simulations of dense gas-solid fluidized bed containing various gas distributors or in the presence of a slotted draft tube. Hosseini et al. [31] found reasonable hydrodynamics simulation results in the dense and dilute regions of a cylindrical spouted bed with a non-porous draft tube using the frictional model of Srivastava and Sundaresan [32]. Azizi et al. [33], Rahimi and Azizi [34] and Shuyan et al. [35] simulated the experiments of Ishikura et al. [36] for a spouted bed with a porous draft tube. They obtained reliable simulation results employing the Srivastava and Sundaresan [32] and Johnson and Jackson [37] frictional stresses models, respectively.

More recently, Hosseini et al. [38] highlighted the influence of frictional stresses on the numerical simulation of a conical spouted bed by evaluating different frictional models including the case that the frictional stress was neglected. They found reliable simulation results using Srivastava and Sundaresan's [32] frictional stress model for α_s^{min}=0.6.

Recently, one of the few two-fluid modelings of vibrated fluidized beds was reported by Acosta-Iborra et al. [39]. In their simulation they solved the two-fluid model equations in a coordinate frame attached to the wall that moves with the vibrating walls of the gas-solid fluidized bed. The sinusoidal vibration was transformed into an acceleration terms that acts like a body force on both the gas and the particle phase equations. Their simulation results showed trends similar to those seen in the discrete particle simulations as well as the experimental data reported for beds containing Geldart group B particles. Recently, Zhang and Ahmadi [40] analyzed three-phase liquid-solid-bubbly flows under microgravity conditions. They also transformed the governing equations to a moving frame and treated the g-jitter acceleration of the column as a body force. Earlier, Ellison et al. [41] studied the motion of particles in a liquid under g-jitter excitation using a similar transformation. They, however, used an idealized fluid model and found a semi-analytical solution for the flow field.

In the present work, TFM based on the kinetic theory of granular flow including the effect of frictional stresses was used for modeling of a vibrating fluidized bed. The simulation procedure followed the approach of Acosta-Iborra et al. [39] with the coordinate transformation to a frame that moves with the vibrating wall. The simulation results were presented in graphical form and discussed. Particular attention was given to the influence of frictional stresses on the hydrodynamic of vibrating fluidized beds.

THEORETICAL TREATMENTS

1. Governing Equations

The Eulerian two-fluid model was used in the present simulation where the two phases are treated as interpenetrating continua [42,43]. The conservation laws for the two phases in a moving frame result in a set of coupled partial differential equations with similar mathematical structure. The corresponding governing equations are:

Continuity equation for phase k (k=g for gas or s for solid phase):

$$\frac{\partial}{\partial t}(\alpha_k \rho_k) + \frac{\partial}{\partial x_i}(\alpha_k \rho_k u_{ki}) = 0 \tag{1}$$

Momentum equations for solid phase in moving frame:

$$\left[\frac{\partial}{\partial t}(\alpha_s \rho_s u_{si}) + \frac{\partial}{\partial x_j}(\alpha_s \rho_s u_{sj} u_{si})\right]$$
$$= -\alpha_s \frac{\partial P_g}{\partial x_i} + \frac{\partial \tau_{sij}}{\partial x_j} + I_{gsi} + \alpha_s \rho_s (g_i - a_w) \tag{2}$$

Momentum equations for gas phase in moving frame:

$$\left[\frac{\partial}{\partial t}(\alpha_g \rho_g u_{gi}) + \frac{\partial}{\partial x_j}(\alpha_g \rho_g u_{gj} u_{gi})\right]$$
$$= -\alpha_g \frac{\partial P_g}{\partial x_i} + \frac{\partial \tau_{gij}}{\partial x_j} - I_{gsi} + \alpha_g \rho_g (g_i - a_w) \tag{3}$$

Here, α_g and α_s are the volume fractions for the gas and solid phases, with the sum of the volume fractions of all phases, is unity. In Eqs. (1)-(3), u_g and u_s are, respectively, the velocity vectors of gas and solid phases with respect to the wall of the fluidized bed, ρ_g stands for the gas phase density and ρ_s is the solid phase density, P_g is the pressure in the fluid phase, a_w is the vertical acceleration of the wall of the bed, and g is the gravitational acceleration. The drag formula is given by the product of the drag interaction term and relative velocity:

$$I_{gsi} = \beta_{gs}(u_{gi} - u_{si}) \tag{4}$$

where β_{gs} is coefficient of the drag term. The drag force acting on the particle phase in two fluid model of gas-solid systems was studied by a number of investigators. Here, the drag model of Gidaspow [44] is used in the analysis. Accordingly,

$$\beta_{gs} = \frac{3}{4} C_D \frac{\alpha_s \alpha_g \rho_g |\mathbf{u}_g - \mathbf{u}_s|}{d_s} \alpha_g^{-2.65} \text{ for } \alpha_g > 0.8 \text{ (Wen-Yu drag model)}$$

$$C_D = \begin{cases} \dfrac{24}{\alpha_g Re_s}[1+0.15(\alpha_g Re_s)^{0.687}], & Re_s < 1000 \\ 0.44 & , Re_s > 1000 \end{cases} ; \ Re_s = \frac{\rho_g d_s |\mathbf{u}_g - \mathbf{u}_s|}{\mu_g}$$

$$\beta_{gs} = 150 \frac{\alpha_s^2 \mu_g}{\alpha_g d_s^2} + 1.75 \frac{\alpha_s \rho_g |\mathbf{u}_g - \mathbf{u}_s|}{d_s} \text{ for } \alpha_g \leq 0.8 \text{ (Ergun drag model)} \tag{5}$$

where d_p, Re_s and C_D stand for the particle diameter, particle Reynolds number and drag coefficient, respectively.

2. Granular Stress Models

Solid stresses in Eq. (2) are given by

$$\tau_{sij} = \left(-P_s + \eta \mu_b \frac{\partial u_{si}}{\partial x_i}\right)\delta_{ij} + 2\mu_s S_{sij} \tag{6}$$

where

$$S_{sij} = \frac{1}{2}\left(\frac{\partial u_{si}}{\partial x_j} + \frac{\partial u_{sj}}{\partial x_i}\right) - \frac{1}{3}\frac{\partial u_{si}}{\partial x_i} \tag{7}$$

Solid pressure:

$$P_s = \alpha_s \rho_s \Theta_s [1 + 4\eta \alpha_s g_0] \tag{8}$$

Solids viscosity:

$$\mu_s = \left(\frac{2+\alpha}{3}\right)\left[\frac{\mu_s^*}{g_0 \eta(2-\eta)}\left(1+\frac{8}{5}\eta \alpha_s g_0\right)\right]$$

$$\times\left(1+\frac{8}{5}\eta(3\eta-2)\alpha_s g_0\right)+\frac{3}{5}\eta\mu_b\right] \tag{9}$$

where

$$\mu_s^* = \frac{\rho_s \alpha_s g_0 \Theta_s \mu'}{\rho_s \alpha_s g_0 \Theta_s + (2\beta_{gs}\mu'/\rho_s \alpha_s)}, \quad \mu' = \frac{5}{96}\rho_s d_s \sqrt{\pi\Theta_s} \tag{10}$$

and

$$\mu_b = \frac{256}{5\pi}\mu'\alpha_s^2 g_0 \tag{11}$$

Solid conductivity of granular energy:

$$\kappa_s = \left(\frac{\kappa_s^*}{g_0}\right)\left[\left(1+\frac{12}{5}\eta\alpha_s g_0\right)\left(1+\frac{12}{5}\eta^2(4\eta-3)\alpha_s g_0\right)\right.$$
$$\left.+\frac{64}{25\pi}(41-33\eta)\eta^2(\alpha_s g_0)^2\right] \tag{12}$$

where

$$\kappa_s^* = \frac{\rho_s \alpha_s g_0 \Theta_s \kappa}{\rho_s \alpha_s g_0 \Theta_s + \left(\frac{6\beta_{gs}\kappa}{5\rho_s\alpha_s}\right)}, \quad \kappa = \frac{75\rho_s d_s\sqrt{\pi\Theta_s}}{48\eta(41-33\eta)} \tag{13}$$

Here, g_0 is the radial distribution function and Θ is the granular temperature. We used the model of Carnahan and Starling [45] for the radial distribution function:

$$g_0 = \frac{1-0.5\alpha_s}{(1-\alpha_s)^3} = \frac{1}{(1-\alpha_s)}+1.5\frac{\alpha}{(1-\alpha_s)^2}+0.5\frac{\alpha_s^2}{(1-\alpha_s)^3} \tag{14}$$

It is noteworthy that Ma and Ahmadi [46] suggested an improved version of the radial distribution function using the second virial theorem. However, this refinement was left for a future study.

In the case with vertical vibration, the granular energy transport equation in the following form is used to solve for Θ:

$$\frac{3}{2}\alpha_s\rho_s\left[\frac{\partial\Theta_s}{\partial t}+u_{sj}\frac{\partial\Theta_s}{\partial x_j}\right]=\frac{\partial}{\partial x_i}\left(\alpha_s\rho_s\kappa_s\frac{\partial\Theta_s}{\partial x_i}\right)$$
$$+\alpha_s\rho_s\tau_{sij}\frac{\partial u_{si}}{\partial x_j}+\Pi_s-\alpha_s\rho_s J_s \tag{15}$$

where the collisional dissipation is given by

$$J_s = \frac{48}{\sqrt{\pi}}\eta(1-\eta)\frac{\alpha_s g_0}{d_s}\Theta_s^{3/2}, \quad \eta = \frac{1+e}{2} \tag{16}$$

and exchange terms are given by [47]

$$\Pi_s = -3\beta_{gs}\Theta_s + \frac{81\alpha_s\mu_g^2|\mathbf{u}_g-\mathbf{u}_s|^2}{g_0 d_s^3\rho_s\sqrt{\pi\Theta_s}} \tag{17}$$

According to previous studies [44,48-51], the algebraic granular temperature is used for the conventional fluidized bed instead of full granular temperature equation that decreases the computational burden without losing accuracy. A conventional fluidized bed is simulated for a qualitative comparison between its results with the CFD results of VFD in terms of solid volume fraction distribution along the bed height. In this study, to evaluate the effects of the additional frictional stresses models on the CFD results of VFD, we used the full granular temperature equation.

2-1. Frictional Stress Models

When particles are closely packed, the effect of frictional stresses becomes quite important. These effects were taken into account in the literature analogous to what was done in soil mechanics, starting from Coulomb friction law [20].

In conventional fluidized beds, the frictional stress model of Schaeffer is used at the critical state, where the solids volume fraction exceeds the maximum packing limit [52]. In the present study, the additional frictional stress model of Srivastava and Sundaresan [32] is used by evaluating different values of minimum concentration for the transition point (α_s^{min}) in simulation of VFB.

In the frictional stress model of Schaeffer, the following relations are used to calculate the solid pressure and viscosity:

$$P_f = P_c = \begin{cases} 10^{25}(\alpha_s-\alpha_s^{max})^{10}, & \alpha_s > \alpha_s^{max} \\ 0 & \alpha_s \le \alpha_s^{max} \end{cases} \tag{18}$$

$$\mu_f = \begin{cases} \min\left(\frac{P_s\sin(\phi)}{\sqrt{4I_{2D}}},\mu_m^{max}\right) & \alpha_s > \alpha_s^{max} \\ 0 & \alpha_s \le \alpha_s^{max} \end{cases} \tag{19}$$

where $\mu_m^{max}=1000$ P.

$$I_{2D} = \frac{1}{6}[(D_{s11}-D_{s22})^2+(D_{s22}-D_{s33})^2+(D_{s33}-D_{s11})^2]$$
$$+D_{s12}^2+D_{s23}^2+D_{s31}^2 \tag{20}$$

and

$$D_{sij} = \frac{1}{2}\left(\frac{\partial u_{si}}{\partial x_j}+\frac{\partial u_{sj}}{\partial x_i}\right) \tag{21}$$

For Srivastava and Sundaresan [32], the following relations are used to calculate the solid pressure and viscosity:

$$P_c = \begin{cases} 10^{25}(\alpha_s-\alpha_s^{max})^{10} & \alpha_s > \alpha_s^{max} \\ Fr\frac{(\alpha_s-\alpha_s^{min})^r}{(\alpha_s^{max}-\alpha_s)^s} & \alpha_s^{max} \ge \alpha_s > \alpha_s^{min} \\ 0 & \alpha_s \le \alpha_s^{max} \end{cases} \tag{22}$$

$$P_f = P_c\left(1-\frac{\nabla\cdot\mathbf{u}_s}{n\sqrt{2}\sin\phi\sqrt{\mathbf{S}:\mathbf{S}+\Theta_s/d_s^2}}\right)^{n-1} \tag{23}$$

$$\mu_f = \frac{\sqrt{2}\sin\phi P_f}{(\sqrt{\mathbf{S}:\mathbf{S}+\Theta_s/d_s^2})}\left(n-(n-1)\left(\frac{P_f}{P_c}\right)^{\frac{1}{n-1}}\right) \tag{24}$$

The value of ϕ for glass is taken to be 28.5° [37]. The frictional stresses start influencing the granular flow at a minimum frictional solids volume fraction (α_s^{min}), which is below the maximum packing (α_s^{max}) as proposed by Johnson and Jackson [53]. In this work, the effect of minimum frictional solids volume fraction is investigated.

In the present study, the modified frictional model of Srivastava and Sundaresan [32] proposed by Benyahia [54] has been used. Fr, r and s are empirical material constants, which, respectively, are taken to be 0.5, 2.0, and 5. The coefficient n is set differently depending on whether the granular assembly experiences a dilatation or compaction:

$$n = \begin{cases} \dfrac{\sqrt{3}}{2\sin\phi} & \nabla \cdot \mathbf{u}_s \geq 0 \\ 1.03 & \nabla \cdot \mathbf{u}_s < 0 \end{cases} \qquad (25)$$

$$\mu_f^{bulk} = -\frac{2}{3}\mu_f \qquad (26)$$

3. Vibrations

It is assumed that the vessel walls are vibrating vertically with the use of a motor. The corresponding sinusoidal vertical vibrations are added to the numerical model of a fluidized bed. The associated displacement Z_w, acceleration a_w, and velocity V_w of the bed are given as,

$$\begin{aligned} Z_W &= A\sin(2\pi ft) \\ a_W &= -(2\pi f)^2 Z_W \\ V_W &= A(2\pi f)\cos(2\pi ft) \end{aligned} \qquad (27)$$

where A, and f are, respectively, the amplitude and frequency of vibration. Note that displacement, velocity and acceleration of the vibrated distributor are as a function of time.

4. Computational Domain and Boundary Conditions

In Fig. 1, displacements of a typical VFB are shown for a complete vibration period. The absolute and moving coordinate systems are displayed in this figure. The absolute coordinate refers to a Cartesian system that is fixed and the vessel moves with respect to this coordinate system (Fig. 1(a)). The moving coordinate system is attached to the vessel wall and moves with the wall (Fig. 1(b)). In the moving coordinate system, the walls are stationary. The velocities of gas and particle phases are described with respect to the moving frame. In this case the acceleration of the frame appears as a body force in the governing momentum balance equations.

The following boundary conditions in the moving frame are used:

- Walls: The walls of a vibrating column act as stationary solid walls for particles and the gas phase. In addition, no slip velocity condition is applied at the wall and the partial slip or the rotational aspects of particles at the wall are neglected.

- Outlet: The open surface at the top of the column is treated as outlet boundary condition.

- Bottom of the bed: It is assumed that a gas distributer with tiny slots is placed at the bottom of the bed. Relative gas velocity ($V_g - V_W$) through the distributor slots that are corrected for the vibration effects are specified as inlet boundary condition.

Since the simulations are performed in the moving frame, the results will provide the velocity relative the vessel wall. To evaluate the absolute velocity and acceleration in the absolute coordinate system, the wall velocity and acceleration (V_W, a_W) need to be added computed relative velocities and accelerations.

5. Model Solution Procedure

Lettieri et al. reported good qualitative agreement between 2D
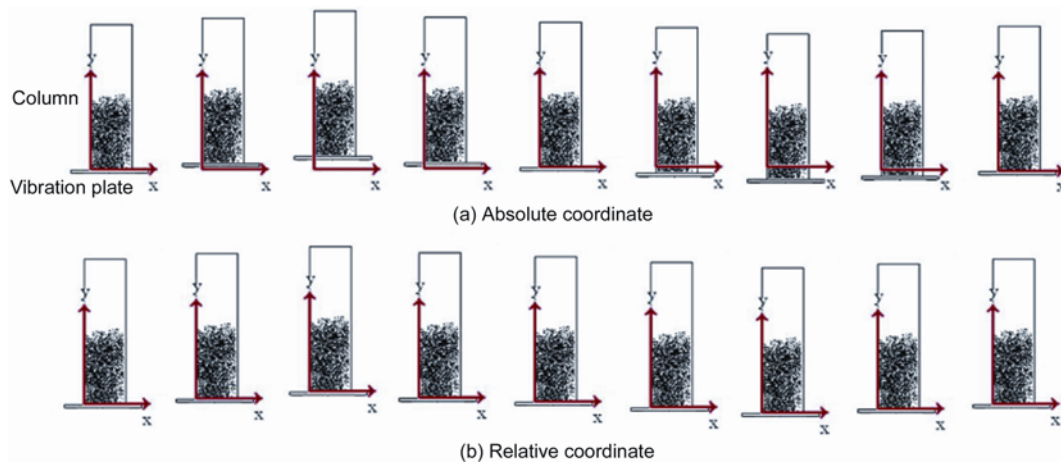
Fig. 1. Different coordinate systems.

Table 1. Boundary conditions and gravity acceleration from the view of different coordinates

Location	Physical property	Absolute coordinate (motional numerical grid)	Relative coordinate (stable numerical grid)
Numerical domain	Gravity acceleration	g	$g - a_w$
BC: Vertical walls	Gas velocity	v_w	Non Slip
	Solid velocity	v_w	Non Slip
	Voidage	$d\alpha_g/dx = 0$	$d\alpha_g/dx = 0$
BC: Column bottom	Gas velocity	Inlet gas velocity	Inlet gas velocity $-v_w$
	Solid velocity	v_w	Non slip
	Voidage	1.0	1.0
BC: Outlet	Gas pressure	P_0	P_0
	Solids velocity	$dv_s/dy = 0$	$dv_s/dy = 0$
	Voidage	$d\alpha_g/dy = 0$	$d\alpha_g/dy = 0$

Table 2. Gas and particle properties for case studies

	Property	Unit	Value
d_s	Particle diameter	μm	1,000
ρ_s	Solids density	kg/m^3	1,050
e	Coefficient of restitution	☐	0.9
ϕ	Angle of internal friction	deg	28.5
α_s^{max}	Maximum solids volume fraction at packing	☐	0.60
α_s^{min}	Minimum solids fraction above which friction sets in	☐	0.45, 0.5, 0.55, 0.60
ρ_g	Gas phase density	kg/m^3	1.185
μ_g	Gas phase viscosity	Pa s	1.14×10^{-5}
U_{mf}	Minimum fluidization velocity	m/s	0.27
U	Superficial inlet gas velocity	m/s	0.5

and 3D simulations of gas-solid fluidized beds, and indicated that 2D models could be used to reduce the computational time with reasonable accuracy [55]. While the full 3D simulation provides greater accuracy, it is computationally intensive and quite time-consuming [56]. In the current study, to keep the computational cost reasonable, along the line of [10-12], a 2D computation model was used.

All simulations of flow condition in a VFB and a conventional fluidized bed are carried out using the MFIX code [57]. The input data used are listed in Table 2.

A 2D computational domain with width and height of 0.025 m and 0.25 m is used for solving the governing equations. The packed bed height is assumed to be 0.055 m. This bed was studied by Xiang et al. [14] using the DEM approach. A computation mesh was developed and the grid independence was tested with varying the grid density of the computational domain. The grid refinement was continued until the solution parameters such as solid volume fraction, gas and solid velocities showed no variations. A computational grid of 6250 cells with a mesh size of about $1.0 \times 1.0 \, mm^2$ was sufficient to guarantee grid independence solutions.

A time duration of 5 s was needed for simulation of VFB to reach steady-state condition. All simulations were continued for 20 s and the time-averaged distributions of flow variables over 5 s to 20 s when the steady state condition was reached were computed. The computational model used an automatic time step adjustment to reduce the run time. This was done with making small increasing or decreasing adjustments in the time step and monitoring the total number iterations for several time steps. The adjustments are continued, if there was a favorable reduction in the number of iterations. Otherwise, adjustments in the opposite direction were attempted. Whenever, the simulation failed to converge, the time step is decreased until convergence was obtained. Typically, an initial time step of 10^{-4} s was used.

RESULTS AND DISCUSSION

### 1. Effects of Frictional Stresses on the Solid Behavior of a VFB

The periodicity contacts of particles and presence of high concentration regions in VFBs were reported in [11,14]. When a dense region of particles occurs, the frictional stresses play an important role and the choice of appropriate frictional stress model significantly affects the accuracy of the simulation results [30,32,38,54,58]. Here,

we used the Srivastava and Sundaresan [32] model, which is expected to be more accurate compared to the other frictional stress models for gas-solid fluidization application. An important parameter of the Srivastava-Sundaresan model is the volume fraction at the transition point for the range that the frictional stresses become important and must be included in the analysis [20,38]. In the subsequent section, the effect of variation in the transition volume fraction is studied. Here, typically a vibration amplitude of 1.0 mm and a vibration frequency of 15 Hz are used. The superficial gas velocity is 0.50 m/s, which is about twice as high as the minimum fluidization velocity in the case without vibration.

As noted before, the magnitude of frictional stress as suggested by the model of Srivastava and Sundaresan [32] varies with the value of minimum solid volume fraction at the transition point, α_s^{min}. Fig. 2 shows the variation of bed height in a VFB for different values of transition solid volume fraction. The bed expansion increases with an increase in the value of α_s^{min}. The particle concentration, however, is highest for smaller α_s^{min} values. The variation of particle concentration with α_s^{min} is highest for large value of α_s^{min}. For low values of α_s^{min}, the variation particle solid volume profile with α_s^{min} is very small as the CFD results for $\alpha_s^{min}=0.45$ and 0.5 are quite consistent. As presented in Eq. (22), the range of applicability of frictional stress
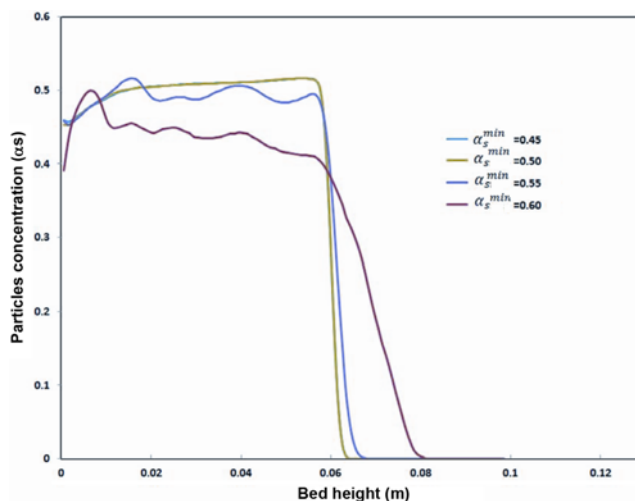
Fig. 2. Effect of frictional stress model on distribution of particle concentration along bed height.
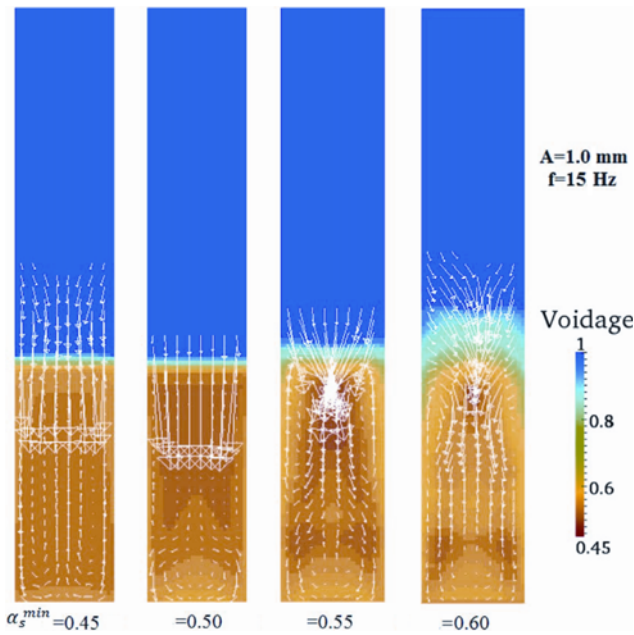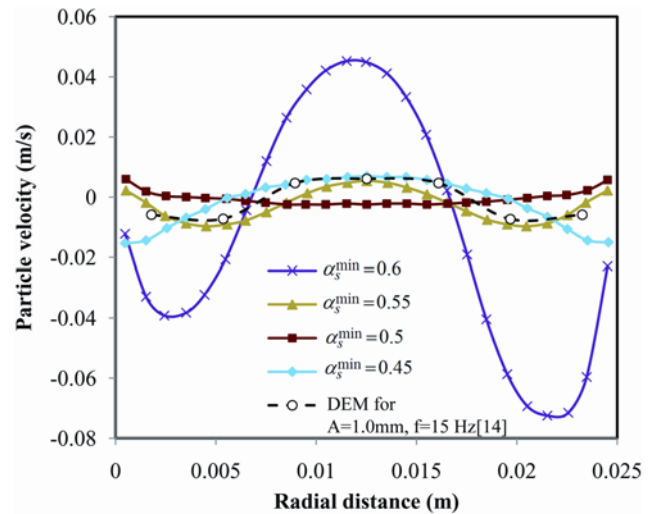
Fig. 3. Effect of frictional stress model on average voidage and particle velocity pattern.

decreases with increasing α_s^{min} values. For simulation of VFBs by TFM inclusion of frictional stress in the model and the use of appropriate values of minimum concentration for the transition point as described by Srivastava and Sundaresan [32] are critical.

When the vessel is vibrating, the distributor will move vertically up and down. The vibration energy will transfer to particles by collisions between the distributor and the particles and by the inter-particle collisions.

The variation in the granular kinetic energy under different vibration conditions produces different states of motion, namely, solid-like state, transition region, and liquid-like state [7]. Fig. 3 shows the voidage contours for different values of α_s^{min} in the VFB. The particle relative velocity vector fields are also shown in this figure. From Fig. 3, liquid like vibration was observed at the upper part of the bed and solid like vibrations are seen at bottom of the granular bed. The transition state is located between these regions. When the frictional stresses are minimum, liquid-like vibration has been extended more than solid-like vibration (α_s^{min}=0.6). It can be seen that different time averaged particles velocity pattern are formed for different α_s^{min}. This is due to change in the direction of particles movement by the vibration effect, as an external agent for different internal frictional forces. In such a condition particles move down but the vibrating distributor pushes them into the opposite direction.

For the case with highest value of minimum concentration for the transition point (α_s^{min}=0.6), the axial velocity of particles near the bottom of the bed is positive in the center of the column and negative near the walls. At the upper part of the bed, the reverse trend is observed. As shown in Fig. 3, with decreasing α_s^{min} particles rise in the central region of the VFB (from bottom of the bed to the top of the bed) and then return near the wall. The particle flow pattern for α_s^{min}=0.45 agrees with the results of previous studies presented in the literature, especially with the DEM results of Xiang et al. [14].

Fig. 4. Effect of frictional stress model on time averaged distribution of axial velocity of particles.

In Fig. 4, the time-averaged axial particle velocity distributions at a height of y=1.75 cm for different values of α_s^{min} are presented. Positive velocities are upward flows, and negative velocities refer to downward flows. Xiang et al. [14] showed that the particle velocity is upward in the central region and downward near the walls. Fig. 4 shows that with decreasing α_s^{min}, different particle velocity patterns are generated. It is seen that by including the effect of frictional stresses, particularly for the case with α_s^{min}=0.45, the TFM simulations are in agreement with DEM results.

Fig. 5 shows the effects of minimum solid concentration for transition point of frictional stress model of Srivastava and Sundaresan [32] on the overall pressure drop of the VFB. In addition, the periodic displacement of the distributor is also shown in this figure. The pressure drop has oscillatory behavior, which is consistent with that predicted by DEM simulations [14]. Fig. 5 also shows that the pressure drop decreases with the decrease in the value of minimum transition solid volume fraction. The lowest time averaged pressure drop
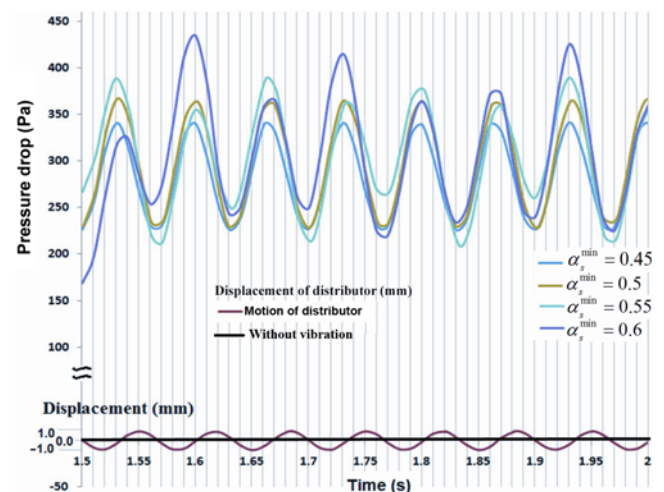
Fig. 5. Effect of frictional stress model on overall pressure drop and displacement of the vibrated distributor as a function of time.
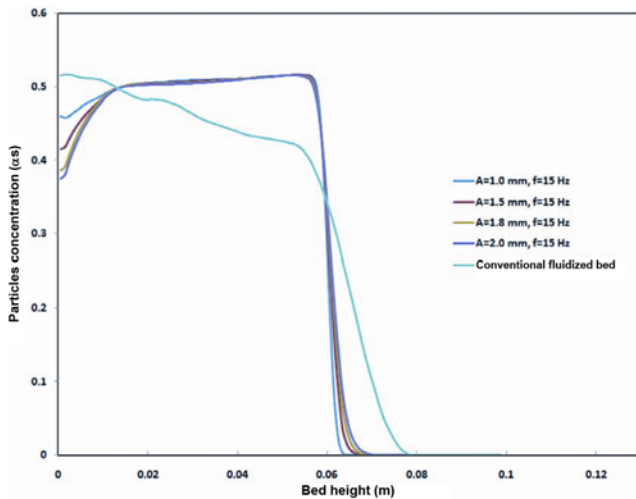
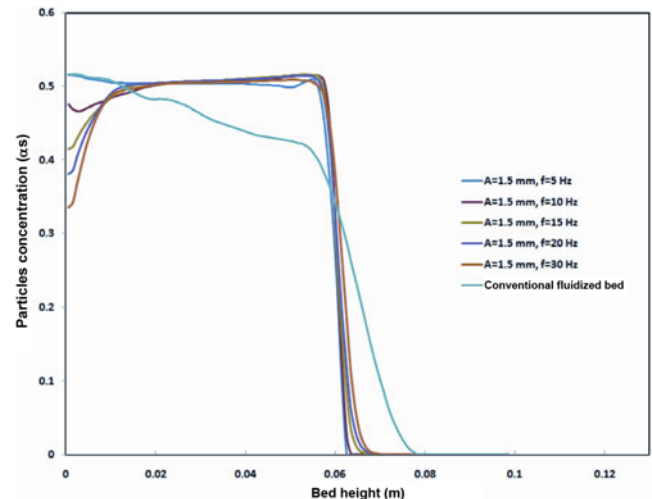**Fig. 6. Influence of vibration amplitude on distribution of particle concentration along bed height.**

Fig. 7. Influence of vibration frequency on distribution of particle concentration along bed height.

is found for α_s^{min}=0.45.

2. Effects of Amplitude and Frequency of Vibration on Solid Behavior

As noted before, the accuracy of numerical simulation depends on the suitable value of transition minimum solid concentration of the frictional stress model of Srivastava and Sundaresan [32]. Section 3.1 suggests that the optimal value is α_s^{min}=0.45. Therefore, this value for the transition minimum solid concentration is used in the rest of simulations. Fig. 6 shows the effect of vibration amplitude on the distribution of time averaged particle concentrations along the bed height. This figure shows that increasing the vibration amplitude (A) leads to reduction of particle concentration near the bottom of bed and increase of bed expansion. When the bed is vibrating, the particle motion along the bed height can be divided into three regimes: a low particle concentration regime near the bottom of the bed, a regime with high concentration in the middle of the bed, and a transition regime at the top of the bed.

For conventional fluidized beds without vibrations, particle concentration highest near the bottom of the bed gradually decreases with the distance from the bottom. For VFB, the decrease of particle concentration near the bottom of bed is due to vibration. In the middle of bed the particle concentration is higher for the case with vibration relative to that without vibration. At the bed top surface, the breakage of gas bubbles causes the reduction in particle concentration. The bed expansion is also higher for the case without vibration compared with the case with vibration.

Fig. 7 shows the effect of vibration frequency (f) on the distribution of particle concentration along the bed height. With increasing vibration frequency, particle concentration is reduced near the bottom of bed and bed expansion is increased. As shown in Fig. 7, the effect of vibration frequency on the particle concentration along the bed is slightly more than that of vibration amplitude. Likewise, three regimes are observed in this figure: low concentration of particles near the bottom, high concentration in the middle of the bed, and a transition regime at the top of the bed.

Fig. 8 shows the time-averaged axial particle velocity for different vibration amplitudes for a fixed vibration frequency of 15 Hz
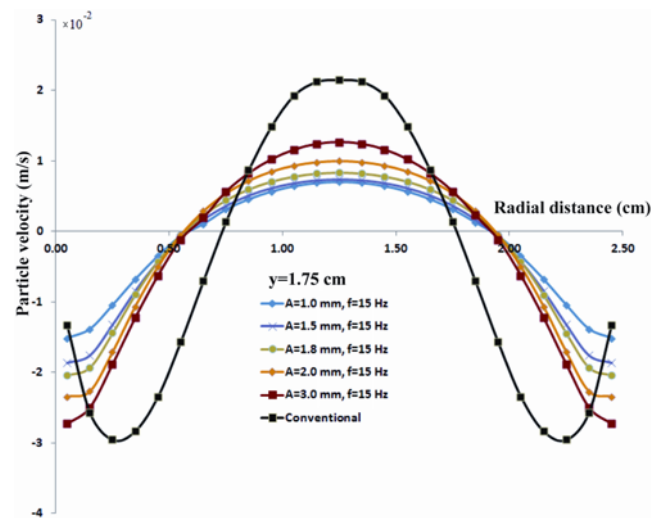

Fig. 8. Time averaged distribution of axial velocity of particles at the different amplitude of vibration.

at y=1.75 cm. The axial velocity of the particles is positive in the central region of the bed and negative near the bed walls, which means particles move upward in the center of the bed and then flow downward near the walls. Therefore, particle circulation is formed in the bed. With increasing the vibration amplitude, the axial velocity of particles increases in the center and is reduced near the walls. Also, the particle velocity profile is more flat for VFB in comparison with the conventional fluidized bed for the same gas injection velocity (U=0.5 m/s). In addition, a conventional fluidized bed predicts higher and lower particle velocity values in the central and near the wall regions, respectively.

Fig. 9 indicates the time-averaged axial velocity of particles for the different vibration frequency and constant vibration amplitude of 1.5 mm at y=1.75 cm. This figure shows that the axial particle relative velocities depend more strongly on the vibration frequency of the bed rather than vibration amplitude. The CFD results for the effects of vibration amplitude and vibration frequency of the bed
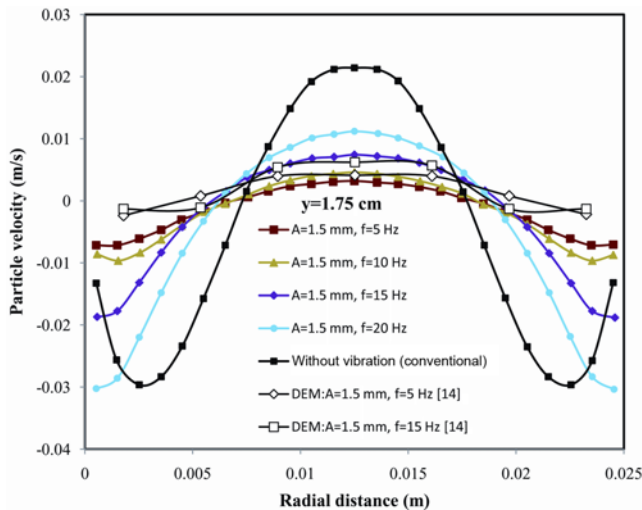
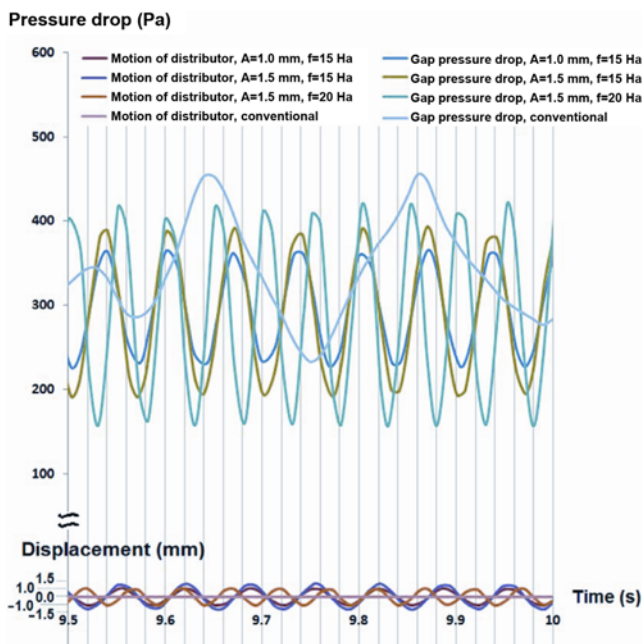**Fig. 9. Time averaged distribution of axial velocity of particles at the different frequency of vibration.**

Fig. 10. Influence of vibration amplitude and frequency on overall pressure drop and displacement of the vibrated distributor as a function of time.

on time averaged axial particle velocity shown in Figs. 8 and 9 are consistent with the results of DEM model of Xiang et al. [14] for the VFBs, especially in the center of the bed. However, the current TFM overpredicts the particle velocity near the wall than that of the DEM results [14].

The overall pressure drops of the VFB and a conventional fluidized bed are evaluated for a range of vibration amplitude and frequencies. Fig. 10 displays the effects of vibration amplitude and frequency on the overall pressure drop versus times. The displacement of the vibrating distributor is also shown for reference. Compared to the case of a conventional fluidized bed in the absence of vibration, more oscillations of the overall pressure drop are seen in

the case of VFB. Also, the computational model predicts that the time-averaged pressure drop of VBF is lower than the conventional fluidized bed. The range of pressure drop oscillations increases with increasing the amplitude of vibration at the same vibration frequency.

A time delay is also observed between maximum and minimum distributor displacement and pressure drop of the VFB. At zero point of wall displacement, the pressure drop is maximum if distributor velocity is positive (at down to up motion) and is minimum if distributor velocity is negative (at up to down motion). These findings confirm the results of Xiang et al. [14] and Tatemoto et al. [11]. Our results show the main oscillation of the pressure curve without local vibration in one cycle. In the previous DEM studies, local vibration of the pressure with time in a one cycle of main pressure oscillation curve was predicted [11,14]. This matter is related to the nature of TFM.

CONCLUSIONS

Using the TFM incorporating the kinetic theory of granular flows, hydrodynamics of a VFB was studied. The governing equations were transformed to a moving frame that is attached to the vibrating wall, with the boundary conditions adjusted accordingly. The simulation results were evaluated in the moving frame. Particular attention was given to the effect of using the frictional stresses on the hydrodynamic of VFB. The model of Srivastava and Sundaresan [32] for the frictional stresses was used in these simulations.

Influences of vibration amplitude and frequency on the motion of particles and solid volume fraction were studied. Both parameters were shown to significantly affect the behavior of solid particles and overall pressure drop of the bed.

The simulation results showed that the overall gas pressure drop exhibited oscillatory trend for VFB, the amplitude of which was higher than that observed for stationary conventional fluidized bed. In addition, current TFM showed the periodicity of displacement of the vibrated distributor with time. The presented simulation results were in agreement with the results of Xiang et al. [14] who have used the DEM computational model.

NOTATION

d_p : particle mean diameter [m]
D : width of the bed (bed diameter) [m]
D_{sij} : rate of strain tensor, solid phase [s^{-1}]
e : restitution coefficient [-]
e_w : particle-wall restitution [-]
g_i : acceleration due to gravity [m/s^2]
g_0 : radial distribution coefficient [-]
H_b : static bed height [m]
I_{2D} : second invariant of the deviator of the strain rate tensor for solid phase [s^{-2}]
I_{gsi} : momentum transfer from fluid phase to solid phase [N/m^3]
J_s : collisional dissipation [m^2/s^3]
P : pressure [Pa]
P_c : critical pressure in solid phase [Pa]
P_f : frictional pressure in solid phase [Pa]
r : radial coordinate [-]
R : radius [-]

Re$_s$: particle Reynolds number [-]
S$_{sij}$: deviatoric part of the rate-of-strain [s^{-1}]
S : deviatoric part of the rate-of-strain tensor [s^{-1}]
t : time [s]
u : velocity vector [m/s]
u$_{ki}$: velocity of phase k [m/s]
u$_s$: tangential velocity of solids [m/s]
U$_g$: superficial gas velocity [m/s]
V$_y$: vertical particle velocity [m/s]
v_{rs} : the ratio of the terminal velocity of a group of particles to that of an isolated particle [-]
y : height measured from distributor [cm]

Greek Letters

α : volume fraction [-]
α_{mf} : gas volume fraction at minimum fluidization [-]
α_s^{max} : maximum solid volume fraction
α_s^{min} : solid fraction at the transition point [-]
β_{gs} : gas/solid momentum exchange coefficient [kg/m^3 s]
δ_{ij} : identity tensor
η : function of restitution coefficient [-]
Θ_s : granular temperature [m^2/s^2]
κ_s : solid conductivity of granular energy [W/m K]
μ : shear viscosity [kg/m s]
Π_s : granular temperature exchange term, [kg/ms^3]
ρ_i : density [kg/m^3]
τ_{kij} : stress tensor of phase k [Pa]
ϕ : angle of internal friction [deg]
ϕ_p : specularity coefficient [-]

Subscripts and Superscripts

g : gas
i, j : indices to identify vector and tensor components
k : phase k, solid or gas
s : solid phase

REFERENCES

1. D. Geldart, *Powder Technol.*, **7**, 285 (1973).
2. Y. Mawatari, T. Koide, Y. Tatemoto, T. Takeshita and K. Noda, *Adv. Powder Technol.*, **12**, 157 (2001).
3. Y. Mawatari, T. Koide, Y. Tatemoto, S. Uchida and K. Noda, *Powder Technol.*, **123**, 69 (2001).
4. S. Mori, A. Yamamoto, S. Iwata, T. Haruta, I. Yamada and E. Mizutani, In: (2nd Ed.), *AIChE Symp. Ser.*, **86**, 88 (1990).
5. Y. Wang, T. Wang, Y. Yang and Y. Jin, *Powder Technol.*, **127**, 196 (2002).
6. L. Zhenfu, F. Maoming, Z. Yuemin, T. Xiuxiang, C. Qingru and C. Zengqiang, *Powder Technol.*, **187**, 119 (2008).
7. T. Shih-Chang and H. Shu-San, *Powder Technol.*, **194**, 159 (2009).
8. Z. Xuejun, Y. Shichao and P. Xiaoheng, *Exp. Therm. Fluid. Sci.*, **32**, 1279 (2008).
9. S. E. Naeini and J. K. Spelt, *Powder Technol.*, **195**, 83 (2009).
10. Y. Tatemoto, Y. Mawatari and K. Noda, *Chem. Eng. Sci.*, **60**, 5010 (2005).
11. Y. Tatemoto, Y. Mawatari, T. Yasukawa and K. Noda, *Chem. Eng. Sci.*, **59**, 437 (2004).
12. M. D. Mantle, A. J. Sederman, L. F. Gladden, J. M. Huntley, T. W. Martin, R. D. Wildman and M. D. Shattuck, *Powder Technol.*, **179**, 164 (2008).
13. Z. Xuejun, Y. Shichao and P. Xiaoheng, *Exp. Therm. Fluid. Sci.*, **32**, 1279 (2008).
14. L. Xiang, W. Shuyan, L. Huilin, L. Goudong, C. Juhui and L. Yikun, *Powder Technol.*, **197**, 25 (2010).
15. B. Ren, W. Zhong, B. Jin, Z. Yuan and Y. Lu, *Energy Fuels*, **25**, 4095 (2011).
16. M. Oevermann, S. Gerber and F. Behrendt, *Particuology*, **7**, 307 (2009).
17. T. Zhao, M. Takei and D.-H. Doh, *Flow Meas. Instrum.*, **21**, 212 (2010).
18. C. H. Ibsen, E. Helland, B. H. Hjertager, T. Solberg, L. Tadrist and R. Occelli, *Powder Technol.*, **149**, 29 (2004).
19. N. G. Deen, M. Van Sint Annaland, M. A. Van der Hoef and J. A. M. Kuipers, *Chem. Eng. Sci.*, **62**, 28 (2007).
20. A. Passalacqua and L. Marmo, *Chem. Eng. Sci.*, **64**, 2795 (2009).
21. W. Zhong, M. Zhang, B. Jin and Z. Yuan, *Powder Technol.*, **175**, 90 (2007).
22. X. Wang, B. Jin and W. Zhong, *Chem. Eng. Process.*, **48**, 695 (2009).
23. J. Wang, W. Ge and J. Li, *Chem. Eng. Sci.*, **63**, 1553 (2008).
24. P. Pei, K. Zhang, J. Ren, D. Wen and G. Wu, *Particuology*, **8**, 425 (2010).
25. S. Vun, J. Naser and P. Witt, *Powder Technol.*, **204**, 11 (2010).
26. L. Huilin, H. Yurong, L. Wentie, D. Jianmin, D. Gidaspow and J. Bouillard, *Chem. Eng. Sci.*, **59**, 865 (2004).
27. W. Shuyan, L. Xiang, L. Huilin, Y. Long, S. Dan, H. Yurong and D. Yonglong, *Powder Technol.*, **196**, 184 (2009).
28. D. J. Patil, M. van Sint Annaland and J. A. M. Kuipers, *Chem. Eng. Sci.*, **60**, 57 (2005).
29. D. J. Patil, M. van Sint Annaland and J. A. M. Kuipers, *Chem. Eng. Sci.*, **60**, 73 (2005).
30. S. H. Hosseini, G. Ahmadi, R. Rahimi, M. Zivdar and M. N. Esfahany, *Powder Technol.*, **200**, 202 (2010).
31. S. H. Hosseini, M. Zivdar and R. Rahimi, *Chem. Eng. Process.*, **48**, 1539 (2009).
32. A. Srivastava and S. Sundaresan, *Powder Technol.*, **129**, 72 (2003).
33. S. Azizi, S. H. Hosseini, M. Moraveji and G. Ahmadi, *Particuology*, **8**, 415 (2010).
34. M. R. Rahimi and S. Azizi, *Chem. Prod. Process Model.*, **6**, 1 (2011).
35. W. Shuyan, L. Yongjian, W. Lixin, D. Qun and W. Chunsheng, *Powder Technol.*, **199**, 238 (2010).
36. T. Ishikura, H. Nagashima and M. Ide, *Powder Technol.*, **131**, 56 (2003).
37. P. C. Johnson, P. Nott and R. Jackson, *J. Fluid Mech.*, **210**, 501 (1990).
38. S. H. Hosseini, G. Ahmadi, B. S. Razavi and W. Q. Zhong, *Energy Fuels*, **24**, 6086 (2010).
39. A. Acosta-Iborra, F. Hernández-Jiménez, M. de Vega and J. V. Briongos, *Chem. Eng. J.*, **261**, 198 (2012).
40. X. Zhang and G. Ahmadi, *J. Comput. Multiphase Flows*, **4**, 41 (2012).
41. J. Ellison, G. Ahmadi, L. Regel and W. Wilcox, *Microgravity Sci. Tec.*, **8**, 140 (1995).
42. D. Ma and G. Ahmadi, *Int. J. Multiphase Flow*, **16**, 341 (1990).
43. G. Ahmadi and D. Ma, *Int. J. Multiphase Flow*, **16**, 323 (1990).

44. D. Gidaspow, *Multiphase flow and fluidization, continuum and kinetic theory descriptions*, Academic Press, Boston (1994).
45. N. F. Carnahan and K. E. Starling, *J. Chem. Phys.*, **51**, 635 (1969).
46. D. Ma and G. Ahmadi, *J. Chem. Phys.*, **84**, 3449 (1986).
47. S. Benyahia, M. Syamlal, T. J. O'Brien, "Summary of MFIX Equations 2012-1." From URL https://mfix.netl.doe.gov/documentation/MFIXEquations2012-1.pdf, January (2012).
48. B. G. M. van Wachem, J. C. Schouten, R. Krishna, C. M. van den Bleek and J. L. Sinclair, *AIChE J.*, **47**, 1035 (2001).
49. A. Boemer, H. Qi and U. Renz, *Int. J. Multiphase Flow*, **23**, 927 (1997).
50. J. Min, J. B. Drake, T. J. Heindel and R. O. Fox, *AIChE J.*, **56**, 1434 (2009).
51. S. Azizi, S.H. Hosseini, G. Ahmadi and M. Moraveji, *Chem. Eng. Technol.*, **33**, 421 (2010).
52. D. G. Schaeffer, *J. Diff. Equ.*, **66**, 19 (1987).
53. P. C. Johnson and R. Jackson, *J. Fluid Mech.*, **176**, 67 (1987).
54. S. Benyahia, *Ind. Eng. Chem. Res.*, **47**, 8926 (2008).
55. P. Lettieri, G. Micale, L. Cammarata and D. Colman, *Computational fluid-dynamics simulations of gas-fluidized beds: A preliminary investigation of different modelling approaches*, In Proceedings of the 10th Germany Workshop on Two-Phase Flow Predictions (2002).
56. F. Bertola, M. Vanni and G. Baldi, *Int. J. Chem. Reactor Eng.*, **1**, A3 (2003).
57. M. Syamlal, W. Rogers, T. J. O'Brien, MFIX documentation: Theory guide, Tech. Rep. DOE/METC-94/1004 (DE9400087), Morgantown Energy Technology Center, Morgantown, West Virginia (1993).
58. S. B. Savage, *J. Fluid Mech.*, **377**, 1 (1998).